Magnetic-nonmagnetic Phase Transition with Interlayer Charge Disproportionation of Nb_3 Trimers in the Cluster Compound Nb_3Cl_8

Yuya Haraguchi[*, †], Chishiro Michioka[†], Manabu Ishikawa[†, ‡], Yoshiaki Nakano[†, ‡], Hideki Yamochi[†, ‡], Hiroaki Ueda[†], and Kazuyoshi Yoshimura[†, ‡, §]

[†]Department of Chemistry, Graduate School of Science, Kyoto University, Kyoto 606-8502, Japan

[‡]Research Center for Low Temperature and Materials Sciences, Kyoto University, Kyoto 606-8501, Japan

[§]Institute for Liberal Arts and Sciences, Kyoto University, Kyoto 606-8501, Japan

ABSTRACT: We have grown large single crystals of the cluster magnet Nb_3Cl_8 with a magnetic triangular lattice, and investigated its magnetic properties and crystal structure. In Nb_3Cl_8, the $[Nb_3]^{8+}$ cluster has a single unpaired spin, making it an S = 1/2 triangular lattice antiferromagnet. At low temperatures, Nb_3Cl_8 exhibits a magnetic-nonmagnetic phase transition driven by a charge disproportionation, in which the paramagnetic $[Nb_3]^{8+}$ clusters transform into alternating layers of nonmagnetic $[Nb_3]^{7+}$ and $[Nb_3]^{9+}$ clusters. The observed exotic phenomenon with the strong correlation between the magnetism and structure are based on the nature of the cluster magnetism.

INTRODUCTION

Cluster units consisting of several ions are occasionally found in inorganic crystal structures. Clusterization occurs for the gain of electron energy to form a large direct overlap among several ions. "Cluster magnets," in which each cluster has unpaired electrons similar to a radical ion, are classified as localized spin systems. Such localization is stabilized by a suitable ratio between the transfer integral and the on-site Coulomb repulsion among clusters. When the optimum ratio is hampered, charge fluctuations within a cluster would be enhanced result in an itinerant system. The charge fluctuation properties are among the important characteristics of cluster magnets, but are absent in the ordinal localized spin systems of magnetic ions. As a result, cluster magnets are expected to produce novel phenomena and have been extensively investigated.[1–7]

Recently, the class of compounds $[A]M_3X_8$ (A = interstitial cations, M = transition metal, X = anion) has attracted the attentions of theorists and experimentalists.[8–14] As shown in Figure 1(a), the M ions form a "breathing" kagomé network, which consists of two kinds of metal triangles with two distinct metal-metal distances. This deformation of the kagomé lattice produces metal-metal bonding in the short trimers owing to the overlap of their orbitals of d electrons, which results in the formation of a cluster-based triangular lattice. Mo_3 cluster compounds typically have the chemical formula $[A]M_3X_8$. These clusters often have $[Mo_3]^{12+}$ and $[Mo_3]^{10+}$ oxidation states, and are nonmagnetic because of the absence of unpaired spins.[9, 15–18] On the other hand, in $LiZn_2Mo_3O_8$, $Li_2ScMo_3O_8$, and $Li_2InMo_3O_8$, since the valence state is $[Mo_3]^{11+}$ with one unpaired spin, each Mo_3 cluster shows S = 1/2 magnetism.[9-11] Indeed, these compounds show the characteristic phenomena of triangular lattice antiferromagnets: valence bond solid formation observed in $LiZn_2Mo_3O_8$, spin liquid condensation in $Li_2ScMo_3O_8$, and magnetic ordering with 120° structure in $Li_2InMo_3O_8$.[9-11]

In this study, we have focused on the $[A]M_3X_8$ type niobium chloride Nb_3Cl_8,[19,20] in which three Nb ions form a Nb_3 trimer resulting in the formation of a Nb_3Cl_{13} cluster unit (Figure 1(b)). Each Nb3 trimer has quite short Nb-Nb intra-cluster distance ($d_{Nb\text{-}Nb}$ ~ 2.8 Å).[20] This fact indicates the formation of metal-metal bondings. In other short Nb-Nb distance compounds, for example, elemental Nb ($d_{Nb\text{-}Nb}$ = 2.853 Å), $LiNbO_2$ ($d_{Nb\text{-}Nb}$ =2.907 Å), NbO_2 ($d_{Nb\text{-}Nb}$ = 2.688 Å), and Nb_6F_{15} ($d_{Nb\text{-}Nb}$ = 2.799 Å), the formation of the metal-metal bondings has been discussed.[21-24] As a result of the metal-metal bondings, the molecular orbitals are formed from three t_{2g} orbitals as depicted in Figure 1(c). Each Nb_3 trimer has seven d electrons yielding a valence state of $[Nb_3]^{8+}$. Thus, the $[Nb_3]^{8+}$ clusters would display S = 1/2 magnetism. This electronic state is similar to the above-mentioned $[Mo_3]^{11+}$ systems. On the other hand, Nb_3Cl_8 exhibits strong lattice instability because the magnetic layers are connected only by weak van der Waals' forces without binding cations (Figure 1(d)). Therefore, Nb_3Cl_8 is expected to display different novel phenomena when compared to the other $[A]M_3X_8$ systems.

In this paper, we report the investigation of the charge disproportionated magnetic-nonmagnetic phase transition at ~100 K in Nb_3Cl_8. We discuss the mechanism of the charge disproportionation based on X-ray diffraction, NMR measurements.

EXPERIMENTAL PROCEDURE

Sample Preparation and Characterization Powders of $NbCl_5$ and elemental Nb were used as starting materials. For the synthesis of the precursor, a mixture of the starting materials with the molar ratio Nb:Cl = 3:8 was calcined in a sealed silica tube under an Ar atmosphere at 700°C for 48h. Single crystals of Nb_3Cl_8 were grown at 750°C for 150h from the precursor powders by the solvent evaporation $PbCl_2$ flux

method. After the growth was complete, the remaining $PbCl_2$ was removed by soaking the crystals in hot water. Powder samples of Nb_3Cl_8 were prepared by sonicating the obtained single crystals, in order to prevent chemical decomposition by the mechanical grinding. The SEM images, obtained by using a SEM/EDS spectrometer (SU1510, HITACHI), reveal that the powder samples consist of a conglomerate of thin nanoscale single crystals (see Figure. S2 in Supporting Information). The samples were characterized by powder X-ray diffraction (XRD) on a diffractometer using Cu Kα radiation.

Measurement of Physical Properties The temperature dependence of the magnetization was measured under several magnetic fields (up to 7T) by using the magnetic property measurement system (MPMS; Quantum Design) at the LTM Research Center, Kyoto University. ^{93}Nb-NMR measurements were carried out by the spin-echo technique with a standard phase-coherent-type NMR-pulsed spectrometer. The ^{93}Nb nucleus with I = 9/2 has a nuclear gyromagnetic ratio γ = 10.407 MHz/T. ^{93}Nb-NMR spectra were recorded by summation of the fast Fourier transform of spin echo signals at several frequencies in the range 60-65 MHz. Typical pulses lengths were 5 and 10μs for the π/2- and π-pulses, respectively, with a pulse separation of τ = 150μs.

Single crystal X-ray diffraction experiment were performed with using Rigaku AFC8 diffractometer equipped with a Eulerian 3 circle CCD detector with Mo $K\alpha$ radiation. Data were collected and processed with solutions and refinements of the crystal structures using the package program of Crystal Clear SM1.3.6 SP3.r6 (Rigaku/MSC Inc., 2006). A plate-like crystal (0.47 × 0.45 × 0.06 mm) was used for single-crystal data analysis. For the low-temperature experiment, a single crystal of Nb_3Cl_8 was glued with epoxy cement on the tip of a quartz fiber and mounted on a goniometer head.

RESULTS AND DISCUSSION

Fine single crystals of Nb_3Cl_8 were successfully grown. As shown in the inset of Figure 2, the obtained single crystals are dark green hexagonal plates with a typical size of 3 × 3 × 0.5 mm. They are strongly cleavable along the *ab*-plane similar to black mica, indicating that the magnetic layers are connected by weak van der Waals' forces. X-ray diffraction patterns (XRD) of the powder and single crystal samples are shown in Figure 2. All peaks of powder sample were indexed to Bragg reflections based on the space group $P\bar{3}m1$, indicating that a single-phase sample was obtained. The XRD pattern of the single crystal was measured in the condition of the scattering vector parallel to 0 0 l. Only 0 0 l diffractions can be obtained without other diffractions, suggesting a single domain crystal.

Figure 3 shows the temperature dependence of the magnetic susceptibility of single crystal and powder samples Nb_3Cl_8 (χ_s and χ_p). There is a large difference between the χ_s and χ_p curves. At T^*~ 100 K, χ_s drops rapidly with a large hysteresis indicating the magnetic phase transition. Below T^*, the value of χ_s approaches to approximately zero, indicating that Nb_3Cl_8 in the low temperature phase is nonmangetic. In a low temperature region, χ_s shows a small Curie tail with sample depending. Such an extrinsic Curie tail is sometimes observed in nonmagnetic compounds including a slight paramagnetic impurity. On the other hand, there is no anomaly at T^* in χ_p, indicating that the phase transition is suppressed in the powder sample. In the high-temperature region, both χ are well fitted to the Curie-Weiss function,

$$\chi = \frac{p_{\mathrm{eff}}^2/8}{T-\theta_{\mathrm{W}}}, \quad (1)$$

where p_{eff} is the effective paramagnetic Bohr magneton and θ_{W} is the Weiss temperature as fitting parameters. They are estimated as p_{eff} = 1.691(9) and θ_{W} = −13.1(3) K. The experimentally obtained value of p_{eff} is consistent with the ideal value of 1.73 for S = 1/2, indicating the existence of one unpaired spin on the molecular orbitals of each Nb_3 trimer. The negative θ_{W} indicates that the magnetic interactions between Nb_3 trimers are dominantly antiferromagnetic. The χ_s curves measured in the parallel and perpendicular fields to the *c*-axis almost coincide, indicating small magnetic anisotropy in Nb_3Cl_8.

Powder samples of Nb_3Cl_8 are in a paramagnetic state down to T ~ 2 K. As mentioned in Sec. IIA, the powder samples consist of a conglomerate of thin single crystals. In addition, a significant broadening of the 0 0 l XRD peaks is observed in powder samples compared with that of the single crystal as (Figure S3 of Supporting Information). We roughly estimated the average thickness of the crystals in the powder samples using the Scherrer formula $L = K\lambda/\beta\cos\theta$, where L is the average crystallite size, λ is the X-ray wavelength, β is the peak width of the diffraction peak profile at half maximum (FWHM) in radians, θ is the Bragg peak position, and K is a constant related to crystallite shape normally taken as 0.9.[25] The estimated average thickness in the powder samples is L = 0.1022 μm. This value is approximately 28×c Nb_3Cl_8 in the low temperature phase of as discussed later. With the reduction in crystal size, stacking faults would be formed simultaneously. As a result, such the decrease of periodicity possibly suppresses the long-range ordering at T^* in the powder samples.

Table 1. Estimated electric quadrupole frequency ν_Q, shift K, asymmetry parameter η, and relative abundance ratio (AO) of the ^{93}Nb-NMR spectra.

Site	ν_Q (MHz)	K(%)	η	AO
Nb1	0.633	0.393	0.011	~0.5
Nb2	0.598	0.386	0.016	~0.5

At low temperatures, χ_p deviates from the Curie-Weiss law, and exhibits a broad peak around 2.5 K suggesting the development of antiferromagnetic correlations. The black solid line in Figure 3 shows the theoretical curve for an S = 1/2 Heisenberg triangular lattice antiferromagnet with the interaction J/k_B = 9.05(2) K.[26] The curve is consistent with the observed χ_p. In the framework of the mean-field theory, when there are only nearest-neighbor couplings with the superexchange interaction J, θ_{W} is given as $-zJS(S+1)/3k_B$. Thus, $\theta_{\mathrm{W}} = -3/2(J/k_B)$ for the S = 1/2 triangular lattice with z = 6. The J/k_B value of 8.7(2) K estimated from the Curie-Weiss temperature is close to the value obtained from the fitting using the triangular lattice model.

In order to clarify the microscopic surroundings of Nb ions in the low temperature phase, we measured the ^{93}Nb-NMR spectra at 78 K by sweeping frequency in a constant external magnetic field of H = 5.9998 T applied parallel to the *c* axis as plotted in Figure 4. When the nuclear spins are in an electric-field gradient (EFG), the NMR spectrum splits due to the nuclear-electric quadrupole interaction. For ^{93}Nb (I = 9/2), the spectrum splits into nine peaks: the central peak (m = −1/2 ⇄ 1/2), two first (m = ±1/2 ⇄ ±3/2), two second (m = ±3/2 ⇄ ±5/2), two third (m = ±5/2 ⇄ ±7/2), and two fourth satellite

peaks (m = ±7/2 ⇄ ±9/2). As shown in the figure, more than 9 peaks are clearly observed. The resonance peaks are interpreted as a superposition of two sets of 9 peaks as shown in the red and blue lines, which suggests the existence of two kinds of Nb sites in the nonmagnetic phase. The fact that the observed peaks have the same approximate interval indicates that the asymmetry parameter $\eta = (V_{xx}-V_{yy})/V_{zz}$, where $V_{\alpha\alpha}$ is the EFG of $\alpha = x, y, z$ directions, is small. In addition, the similar intensities of both sets suggest that the stoichiometric ratio of two Nb sites is equal in the low temperature phase. TABLE I shows the NMR parameters for both Nb sites; the electric-quadrupole frequency ν_Q, the shift from ideal value K, and η. The dominant contribution to the observed shift K is from the chemical shift, since the single crystal Nb_3Cl_8 is nonmagnetic in the low-T phase. Since the EFG is proportional to $\nu_Q = 3e^2qQ/2hI(2I-1)$, the different ν_Q values for Nb1 and Nb2 indicate that the EFGs of the two Nb sites are different, possibly implying differently distorted $NbCl_6$ octahedra.

Figure 5 shows the determined crystal structure for the single crystal Nb_3Cl_8 at 300 (left) and 24 K (right) (details are shown in TABLE S1 of Supporting Information). The structure at 300 K is consistent with that of the previous report.[20] We found that the structural phase transition occurred at T^* from $P\bar{3}m1$ to $R3$ with a $1a \times 1b \times 3c$ supercell in the trigonal structure. Along with the structural phase transition, the stacking pattern of Nb_3Cl_8 layers also changes, that is, double planes are layered with a shifting of [1/3, −1/3, 0] per unit cell of the high temperature phase (see Figure S1 in Supporting Information). Such the unconventional structural transition could be suppressed by the decrease of structural periodicity in the structure, which is observed in the powder samples. In addition, the stoichiometric ratio of the two Nb sites is equal in the low temperature phase, which is consistent with the result of the NMR investigation. At T^*, the uniform Nb_3 trimers with the same $d_{Nb\text{-}Nb}$ (2.8109(9) Å at 300 K) are divided into two kinds of trimers with different $d_{Nb\text{-}Nb}$ ($d_{Nb1\text{-}Nb1}$= 2.801(3)es Å, $d_{Nb2\text{-}Nb2}$= 2.8207(17) Å at 24 K). Note that the transformation occurs while maintaining the point group (C_{3v}) of the Nb_3 trimers. Each Nb_3 trimer with the same Nb-Nb bond length is arranged on a layer, and the two kinds of the layers are stacked alternately.

Table 2. Intra-cluster Nb-Nb bond length $d_{Nb\text{-}Nb}$, average Nb-Cl bond length $\langle d_{Nb\text{-}Cl}\rangle$, quadratic elongation $\langle\lambda\rangle$, and bond angle variance σ for the $NbCl_6$ octahedra in Nb_3Cl_8 at 300 and 24 K.

T (K)	Site	$d_{Nb\text{-}Nb}$ (Å)	$\langle d_{Nb\text{-}Cl}\rangle$ (Å)	$\langle\lambda\rangle$	σ (°)
300	Nb	2.8109(9)	2.499(1)	1.0268(4)	9.68(4)
24	Nb1	2.801(3)	2.492(2)	1.0250(6)	9.29(6)
24	Nb2	2.8207(17)	2.507(2)	1.0285(8)	10.04(7)

The deviation in the shift of the Nb ions from the center of $NbCl_6$ octahedra results in different degrees of distortion in each $NbCl_6$ octahedron. As a scale-parameter of distortion of octahedra, we introduce two parameters. The quadratic elongation is defined as,

$$\langle\lambda\rangle = \sum_{i=1}^{6} \frac{l_i/l_0}{n}, \quad (2)$$

where n is the coordination-number of anions around the central cation, l_i is the bond length between the central cation and the i-th coordinating anions, and l_0 is the bond length in a polyhedron with O_h symmetry whose volume is equal to that of the distorted one. The bond angle variance is expressed as,

$$\sigma = \sqrt{\sum_{i=1}^{12} \frac{(\varphi_i-\varphi_0)^2}{m-1}}, \quad (3)$$

where m is the number of anion-cation-anion bond angles, ϕ_i is the i-th bond angle of the distorted coronation-polyhedra, and ϕ_0 is the bond angle of the coordination-polyhedra with O_h symmetry.[27] The parameters $\langle\lambda\rangle$ and σ represent the deviation of each bond length of Nb-Cl and bond angle of Cl-Nb-Cl, respectively. Using these parameters, the degree of the deviation in the $NbCl_6$ octahedra can be evaluated. TABLE 2 shows the estimated $\langle\lambda\rangle$ and σ for each $NbCl_6$ octahedron in the high- and low-temperature phases. The values of both parameters in the shrunk Nb1 trimers increase, while the values in the expanded Nb2 trimers decrease. The $\langle\lambda\rangle$ and σ values directly relate to EFG. Thus, the different $\langle\lambda\rangle$ and σ values for the Nb1 and Nb2 sites are consistent with the ^{93}Nb-NMR results.

The phase transition accompanied by the expansion and shrinking of the Nb_3 trimers at T^* can be explained by the charge disproportionation model as schematically described in Figure 6. In the high-temperature phase, the valence state of the uniform Nb_3 trimers is $[Nb_3]^{8+}$ with seven 4d electrons. In this state, each Nb_3 trimer exhibits S = 1/2 magnetism. However, when the Nb_3 trimers undergo charge disproportionation into $[Nb_3]^{7+}$ and $[Nb_3]^{9+}$, they become nonmagnetic due to the absence of unpaired spins. In this way, the observed magnetic-nonmagnetic phase transition at T^* could be described by $2[Nb_3]^{8+} \rightarrow [Nb_3]^{7+} + [Nb_3]^{9+}$. The average length of the Nb-Cl bond $\langle d_{Nb\text{-}Cl}\rangle$ in the $NbCl_6$ octahedron is expected to increase along with the valence of Nb. As shown in the TABLE 2, $\langle d_{Nb1\text{-}Cl}\rangle$ shrinks from 2.499 to 2.492 Å and $\langle d_{Nb2\text{-}Cl}\rangle$ expands from 2.499 to 2.507 Å. This change of the bond lengths is consistent with the charge disproportionation model.

The expansion/shrinking of the cluster bonding length increases/decreases the energy level of the bonding $2a_1$ orbital (see the schematic view of $2a_1$ molecular orbital of the Nb_3 trimer, right side, Figure 7). In the $[Nb_3]^{8+}$ cluster, the $2a_1$ orbital is occupied by a single d electron. During the oxidization ($[Nb_3]^{8+} \rightarrow [Nb_3]^{9+}$), the $2a_1$ orbital becomes unoccupied, while reduction ($[Nb_3]^{8+} \rightarrow [Nb_3]^{7+}$) results in a fully occupied. In the expanded $(Nb1)_3$ trimers and shrunk $(Nb2)_3$ trimers, the energy level of the bonding $2a_1$ decreases and increases, respectively. Therefore, from the point of view of the energy level, the magnetic-nonmagnetic phase transition occurs with the occupation-energy-gain. The energy-dropping $2a_1$ orbital of the Nb1 site becomes fully occupied and the energy-dropping $2a_1$ orbital of the Nb2 site becomes unoccupied (left side, Figure 7. Thus, the observed expansion/shrinking of the cluster bonding strongly demonstrates the charge disproportionation induced by interlayer charge transfer.

Finally, we discuss the origin of the charge disproportionated magnetic-nonmagnetic phase transition. The observed large hysteresis appearing in the cooling and heating processes suggest the strong first-order phase transition, suggesting that the charge disproportionation is not caused by an order-disorder transition of charge or magnetic fluctuation but by the structural phase transition. Thus, it is concluded that the origin of the unconventional phase transition is a lattice instability accompanied by the charge disproportionation, which is also probed by the size effect to suppress the phase transition.

CONCLUSIONS

We have succeeded in growing fine single crystals of the cluster magnet Nb_3Cl_8 by the flux method using the solvent evaporation technique and identified the magnetic-nonmagnetic phase transition at ~100 K. XRD and NMR analyses revealed that the magnetic-nonmagnetic phase transition is driven by a charge disproportionation from layers of paramagnetic $[Nb_3]^{8+}$ to alternating layers of nonmagnetic $[Nb_3]^{7+}$ and $[Nb_3]^{9+}$. Moreover, nanoscale size controlling is found to the suppresses the magnetic-nonmagnetic phase transition. We believe that the unconventional interlayer charge disproportionation is caused by characteristics of the cluster magnets.

ASSOCIATED CONTENT

Supporting Information. Results of refined structural parameters of the single crystal at 300 K and 24 K, SEM images of the powder samples, and X-ray diffraction near the 0 0 2 peaks for single crystal and powder samples. These materials are available free of charge via the Internet at http://pubs.acs.org.

AUTHOR INFORMATION

Corresponding Author

*chiyuya@kuchem.kyoto-u.ac.jp

Notes

The authors declare no competing financial interest.

ACKNOWLEDGMENT

This work is supported by Grant-in-Aids for Scientific Research from MEXT of Japan [Grants No.16H04131 and No.26410089]. Y. H. is supported by Research Fellow of Japan Society for the Promotion of Science [Grants No. 16J04048]

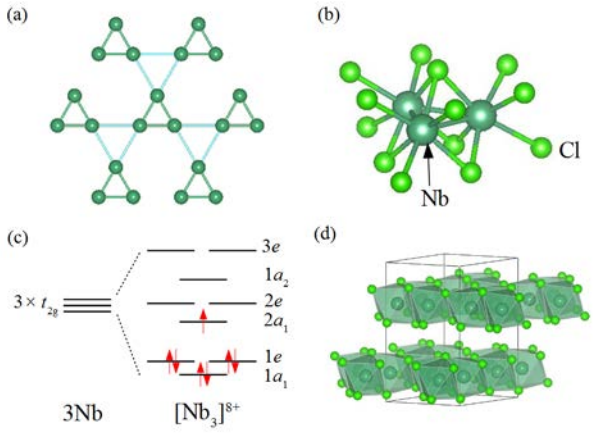

Figure 1. (a) Transition metal trimers forming the triangular lattice. (b) Nb_3Cl_{13} cluster unit. (c) Schematic view of the molecular orbitals formed in a Nb_3 trimer with the ground state electron configuration. (d) Stacking layer structure of Nb_3Cl_8.

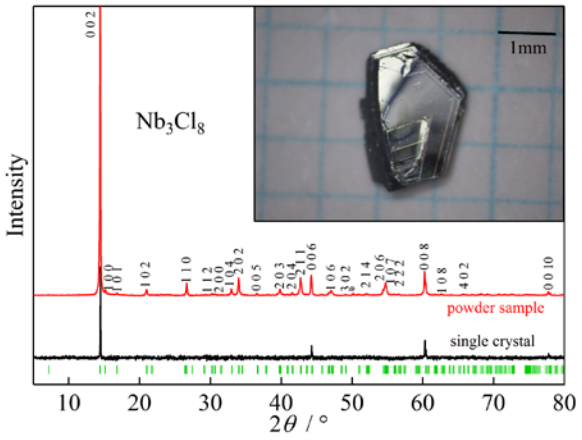

Figure 2. X-ray diffraction patterns of the single crystal and powder samples of Nb_3Cl_8. Vertical bars at the bottom indicate the positions of Bragg reflections, and the Miller indices are indicated in the plot. The inset shows a typical single crystal.

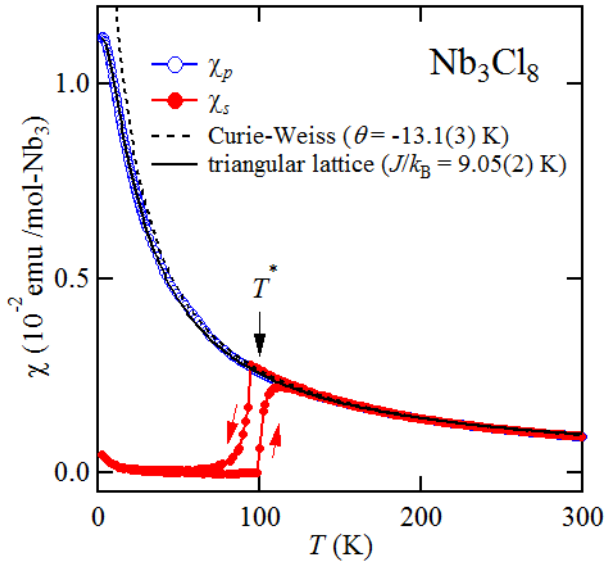

Figure 3. Temperature dependence of the magnetic susceptibilities of single crystal (χ_s, red circles) and powder (χ_p, black circles) samples of Nb_3Cl_8.

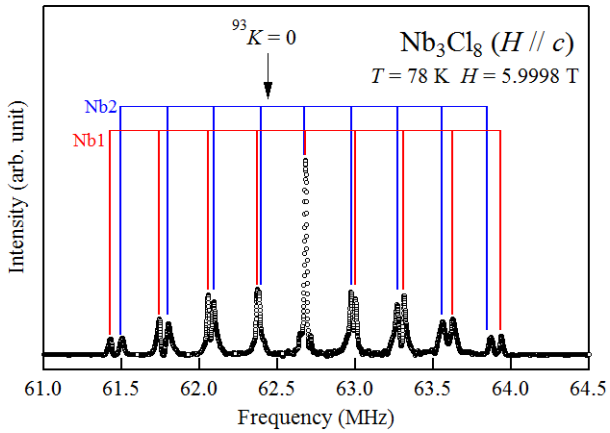

Figure 4. ^{93}Nb-NMR spectrum at T = 78 K and H = 5.9998 T. The resonance peaks are interpreted as a superposition of two sets of nine equally separated peaks, indicating the existence of two Nb sites named Nb1 and Nb2.

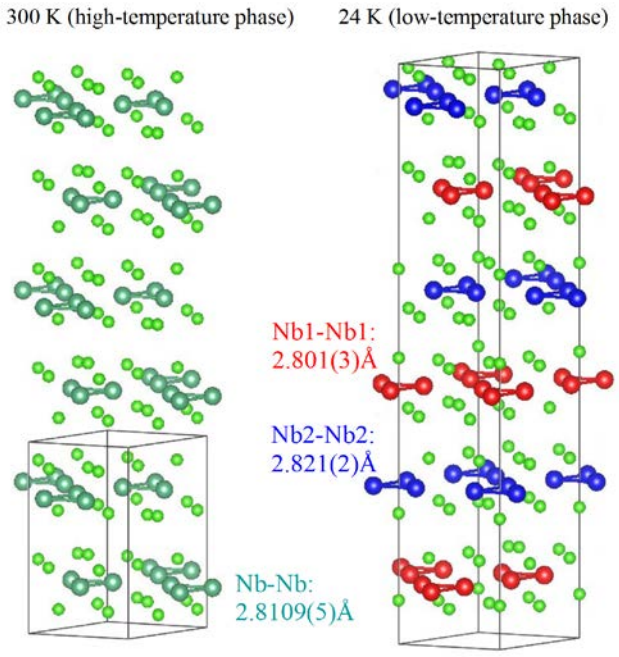

Figure 5. Crystal structures of Nb_3Cl_8 at 300 K (left) and 24 K (right). The Nb-Nb bond lengths within the Nb_3 trimers are indicated.

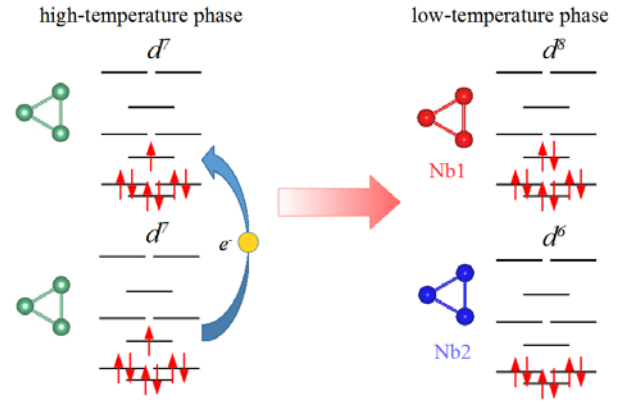

Figure 6. Schematic view of the charge disproportionation of the Nb_3-trimers at $T^* = 100$ K in Nb_3Cl_8.

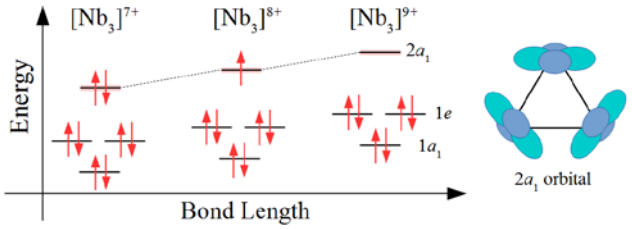

Figure 7. The left side shows the schematic view of energy levels in the bonding orbitals of $[Nb_3]^{n+}$ trimers (n = 7,8,9) with corresponding bond lengths and with their electron configurations. The right side shows a schematic view of the $2a_1$ molecular orbital of the Nb_3 trimer.

REFERENCES

(1) Abd-Elmeguid, M.; Ni, B.; Khomskii, D.; Pocha, R.; Johrendt, D.; Wang, X.; Syassen, K. Transition from Mott Insulator to Superconductor in $GaNb_4Se_8$ and $GaTa_4Se_8$ under High Pressure. *Phys. Rev. Lett.* **2004**, *93*, 126403.

(2) Pocha, R.; Johrendt, D.; Pöttgen, R. Electronic and Structural Instabilities in GaV_4S_8 and $GaMo_4S_8$. *Chem. Mater.* **2000**, *12*, 2882-2887.

(3) Nakamura, H.; Chudo, H.; Shiga, M. Structural transition of the tetrahedral metal cluster nuclear magnetic resonance study of GaV_4S_8. *J. Phys.: Condens. Matter* **2005**, *17*, 6015.

(4) Cuthbert, H.; Greedan, J.; Vargas-Baca, I.; Derakhshan, S.; Swainson, I. Synthesis, Structure, and Unexpected Magnetic Properties of $La_3Re_2O_{10}$. *Inorg. Chem.* **2007**, *46*, 8739-8745.

(5) Haraguchi, Y.; Michioka, M.; Ueda, H.; Yoshimura, K. Unconventional multicritical point in the S=1/2 Re_2-cluster magnet $La_3Re_2O_{10}$. *Phys. Rev. B* **2014**, *90*, 064403.

(6) Miiller, W.; Avdeev, M.; Zhou, Q.; Kennedy, B. J.; Sharma, N.; Ling, C. D. Giant Magnetoelastic Effect at the Opening of a Spin-Gap in $Ba_3BiIr_2O_9$. *J. Am. Chem. Soc.* **2012**, *134*, 3265-3270.

(7) Tran, T. T.; Gooch, M.; Lorenz, B.; Litvinchuk, A. P.; Sorolla, M. G., II; Brgoch, J.; Chu, P. C. W.; Guloy, A. M. $Nb_2O_2F_3$: A Reduced Niobium (III/IV) Oxyfluoride with a Complex Structural, Magnetic, and Electronic Phase Transition. *J. Am. Chem. Soc.* **2015**, *137*, 636-639.

(8) Flint, R.; Lee, P. A. Emergent honeycomb lattice in $LiZn_2Mo_3O_8$. *Phys. Rev. Lett.* **2013**, *111*, 217201.

(9) Torardi, C. C.; McCarley, R. E. Synthesis, crystal structures, and properties of $LiZn_2Mo_3O_8$, $Zn_3Mo_3O_8$, and $ScZnMo_3O_8$, reduced derivatives containing the Mo_3O_{13} cluster unit. *Inorg. Chem.* **1985**, *24*, 476-481.

(10) Haraguchi, Y.; Michioka, C.; Imai, M.; Ueda, H.; Yoshimura, K. Spin-liquid behavior in the spin-frustrated Mo 3 cluster magnet $Li_2ScMo_3O_8$ in contrast to magnetic ordering in isomorphic $Li_2InMo_3O_8$. *Phys. Rev. B* **2015**, *92*, 014409.

(11) Gall, P.; Orabi, R. A. R. A.; Guizouarn, T.; Gougeon, P. Synthesis, crystal structure and magnetic properties of Li_2InMo_3O8: A novel reduced molybdenum oxide containing magnetic Mo_3 clusters. *J. Solid State Chem.* **2013**, *208*, 99-102.

(12) Sheckelton, J. P.; Neilson, J. R.; Soltan, D. G.; McQueen, T. M. Possible valence-bond condensation in the frustrated cluster magnet $LiZn_2Mo_3O_8$. *Nat. Mater.* **2012**, *11*, 493.

(13) Sheckelton, J. P.; Foronda, F. R.; Pan, L. D.; Moir, C.; McDonald, R. D.; Lancaster, T.; Baker, P. J.; Armitage, N. P.; Imai, T.; Blundell, S. J.; McQueen, T. M. Local magnetism and spin correlations in the geometrically frustrated cluster magnet $LiZn_2Mo_3O_8$. *Phys. Rev. B* **2014**, *89*, 064407.

(14) Mourigal, M.; Fuhrman, W. T.; Sheckelton, J. P.; Wartelle, A.; Rodriguez-Rivera, J. A.; Abernathy, D. L.; McQueen, T. M.; Broholm, C. L. Molecular Quantum Magnetism in $LiZn_2Mo_3O_8$. *Phys. Rev. Lett.* **2014,** *112*, 027202.

(15) McCarroll, W.H.; Katz, L.; Ward, R.; Some Ternary Oxides of Tetravalent Molybdenum[1,2]. *J. Am. Chem. Soc.* **1957**, *79*, 5410-5414.

(16) McCarroll, W.H. Structural Relationships in $ARMo_3O_8$ Metal Atom Cluster Oxides. *Inorg. Chem.* **1977**, *16*, 3351-3353.

(17) Gall, P.; Orabi, R. A. R. A.; Guizouarn, T.; Cuny, J.; Fontaine, B.; Gautier, R.; Gougeon, P. *J.* Synthesis, crystal and electronic structures and magnetic properties of $Li_2SnMo_3O_8$: A novel reduced molybdenum oxide containing Mo_3O_{13} cluster units. *Solid State Chem.* **2013,** *201*, 312-316.

(18) Gall, P.; Gougeon, P. $Li_2GeMo_3O_8$: a novel reduced molybdenum oxide containing Mo_3O_{13} cluster units. *Acta Cryst*. **2016,** E72, 995-997.

(19) Cotton, F. A.; Diebold, M. P.; Roth, W. J. Discrete trinuclear complexes of niobium related to the local structure in Nb_3Cl_8. *J. Am. Chem. Soc.* **1987,** *109*, 2833-2834.

(20) Ströbele, M.; Glaser, J.; Lachgar, A.; Meyer, H.-J. Struktur und elektrochemische Untersuchung von Nb_3Cl_8. *Z. Anorg. Allg Chem.* **2001**, *627*, 2002.

(21) Edwards, J. W.; Speiser, R.; Johnston, H. L. High Temperature Structure and Thermal Expansion of Some Metals as Determined by X-Ray Diffraction Data. I. Platinum, Tantalum, Niobium, and Molybdenum *J. Appl. Phys.* **1951**, *22*, 424.

(22) Roth, H. F.; Meyer, G.; Hu, Z.; Kaindl, G. Z. Synthesis, structure, and X-ray absorption spectra of Li_xNbO_2 and Na_xNbO_2 ($x \leq 1$). *Z. Anorg. Allg. Chem.* **1993**, *619*, 1369.

(23) Pynn, R.; Axe, J. D.; Thomas, R. Structural distortions in the low-temperature phase of NbO_2. *Phys. Rev. B* **1976**, *13*, 2965.

(24) Knoll, R.; Sokolovski, J.; BenHaim, Y.; Shames, A. I.; Goren, S. D.; Shaked, H.; Thépotc, J.-Y.; Perrin, C.; Cordier, S. Magnetic resonance and structural study of the cluster fluoride Nb_6F_{15}. *Physica B: Condens. Matter* **2006**, *381*, 47.

(25) Scherrer, P.; Gottingen, N.G.W. Determination of the size and internal structure of colloidal particles using X-rays. *Math-Pys. Kl.* **1918** *2*, 96-100.

(26) Tamura, M.; Kato, R. Magnetic susceptibility of β'-$[Pd(dmit)_2]$ salts (dmit = 1, 3-dithiol-2-thione-4, 5-dithiolate, C_3S_5): evidence for frustration in spin-1/2 Heisenberg antiferromagnets on a triangular lattice. *J. Phys.: Condens. Matter* **2002**, *14*, L729.

(27) Robinson, K.; Gibbs, G. V.; Ribbe, P. H. Quadratic elongation: a quantitative measure of distortion in coordination polyhedra. *Science* **1971**, *172*, 567-570.

Supporting Information
Magnetic-nonmagnetic Phase Transition with Interlayer Charge Disproportionation of Nb_3 Trimers in a Cluster Compound Nb_3Cl_8

Yuya Haraguchi[1,*], Chishiro Michioka[1], Manabu Ishikawa[1,2], Yoshiaki Nakano[1,2], Hideki Yamochi[1,2], Hiroaki Ueda[1], and Kazuyoshi Yoshimura[1,2,3]

[1]Department of Chemistry, Graduate School of Science, Kyoto University, Kyoto 606-8502, Japan
[2]Research Center for Low Temperature and Materials Sciences, Kyoto University, Kyoto 606-8501, Japan
[3]Institute for Liberal Arts and Sciences, Kyoto University, Kyoto 606-8501, Japan
[*]chiyuya@kuchem.kyoto-u.ac.jp

Contents

1 Structural Study

Table S1: Refined Structural Parameters of single crystal Nb_3Cl_8 at 300 and 24 K. Their space groups are $P\bar{3}m1$ and $R3$, respectively for 300 and 24 K. The obtained lattice parameters are $a = 6.7487$ and 12.2853 Å and $c = 6.74$ and 36.75 Å, respectively, for 300 and 24 K. The reliable factors R are 0.0429 and 0.0515, respectively, for 300 and 24 K. SOF stands for site ocupancy factor.

temperature	atom	site	x	y	z	$U(\text{Å}^{-1})$	SOF
300 K	Nb1	6i	0.52783(8)	$1-x$	0.25305(6)	0.0064(3)	1
	Cl1	2d	1/3	2/3	0.1438(3)	0.0095(8)	1
	Cl2	2d	2/3	1/3	0.4013(3)	0.0093(8)	1
	Cl3	6i	0.1645(2)	0.3291(5)	0.3630(2)	0.0113(5)	1
	Cl4	6i	0.8319(2)	0.6638(5)	0.12012(19)	0.0120(5)	1
24 K	Nb1	9b	0.1395(2)	0.2790(2)	0.27451(2)	0.0040(4)	1
	Nb2	9b	0.19477(19)	0.3896(2)	0.1107(2)	0.0018(2)	1
	Cl1	3a	1/3	2/3	0.31318(17)	0.0047(11)	1
	Cl2	9b	0.5037(6)	$1-x$	0.2370(10)	0.0035(6)	1
	Cl3	9b	0.3354(8)	0.1676(6)	0.1464(1)	0.0064(7)	1
	Cl4	3a	0	0	0.2253(2)	0.0047(12)	1
	Cl5	3a	1/3	2/3	0.15995(19)	0.0036(12)	1
	Cl6	9b	0.0033(7)	0.5019(6)	0.06530(9)	0.0020(6)	1
	Cl7	9b	0.8329(7)	0.1668(7)	0.31834(9)	0.0071(7)	1
	Cl8	3a	0	0	0.075339(16)	0.0015(10)	1

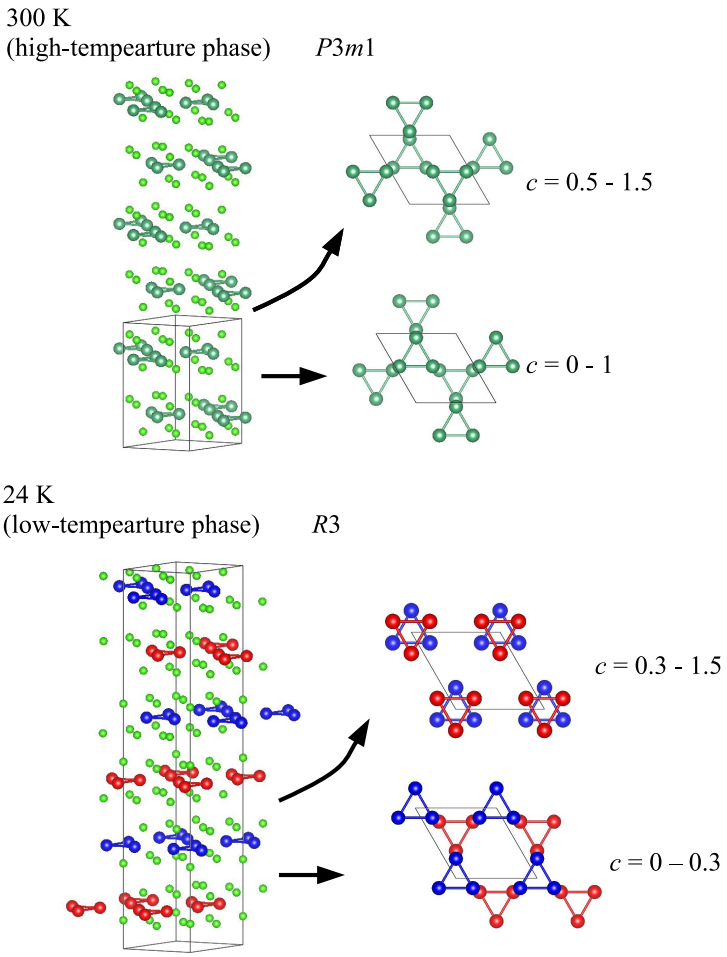

Figure S1: (Color online) Difference of the stacking pattern caused by a stacking shift of the Nb_3Cl_8 at 300 K (left) and 24 K (right).

2 Microscopic Size Evaluation

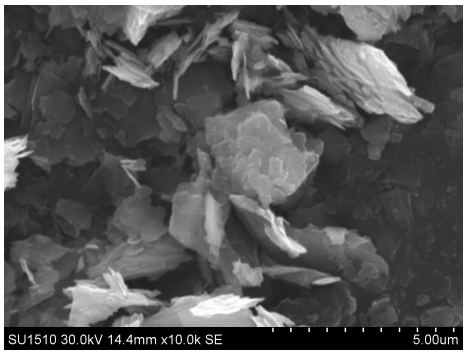

Figure S2: SEM photographs of powder sample of Nb_3Cl_8.

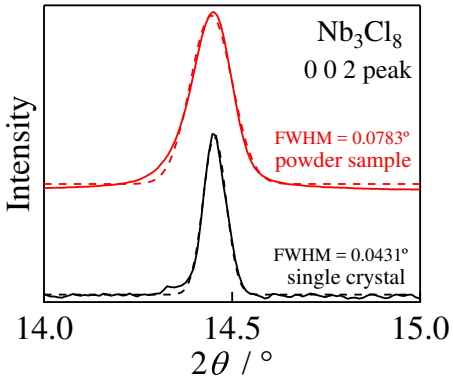

Figure S3: (Color online) Comparison of the effect of crystal size dependence on the 002 peak for single crystal and powder samples of Nb_3Cl_8.

Exotic charge disproportionation is found in a cluster compound Nb_3Cl_8. The charge disproportionation drastically changes the magnetic system from paramagnetic to nonmagnetic. Detailed studies of structure and magnetic properties revealed the origin being the interlayer charge transfer, which results in the unconventional charge arrangement from layers of the paramagnetic $[Nb_3]^{8+}$ to alternating layers of nonmagnetic $[Nb_3]^{7+}$ and $[Nb_3]^{9+}$.

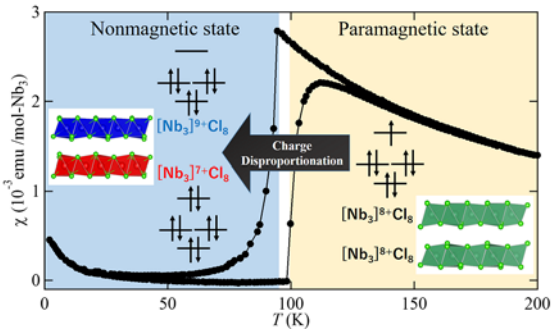

For Table of Contents Only